INTERNATIONAL TRANSACTIONS IN OPERATIONAL RESEARCH

WILEY

INTERNATIONAL TRANSACTIONS IN OPERATIONAL RESEARCH

Intl. Trans. in Op. Res. 33 (2026) 1157–1185
DOI: 10.1111/itor.13539

A bilevel approach to reduce peak load of community microgrid with distributed generators

Young-Bin Woo[a] and Ilkyeong Moon[a,b,*]

[a] *Department of Industrial Engineering, Seoul National University, Gwanak-ro 1, Gwanak-gu, Seoul 08826, Republic of Korea*
[b] *Institute of Engineering Research, Seoul National University, Gwanak-ro 1, Gwanak-gu, Seoul 08826, Republic of Korea*
E-mail: ybwoo@snu.ac.kr [Woo]; ikmoon@snu.ac.kr [Moon]

Received 3 March 2023; received in revised form 24 July 2024; accepted 13 August 2024

Abstract

Decentralized energy systems can be an alternative to stabilizing the power system in a rapidly changing power market environment. In this regard, it is very important to level the significant gap between electricity loads and power generation, which is caused by expanding renewable energy resources. This study investigates an electricity control strategy to encourage forming a microgrid and to level the load profile that the microgrid optimizes based on its individual objective. To address the problems encountered by two players at different decision levels, this study introduces a bilevel optimization model that considers two players' objectives. In the proposed model, the first player is called the grid system operator, and the decisions of the player are subsidy rates for distributed generators and an energy storage system. The second player is called the community microgrid, and the major decisions of the player are the configuration and operation of the microgrid. To solve the problem, an efficient algorithm is developed based on Karush–Kuhn–Tucker (KKT) conditions and a decomposition approach. Numerical experiments show that the peak load can be reduced by setting an adequate subsidy rate.

Keywords: bilevel programming; decomposition algorithm; distributed generator; energy scheduling; microgrid; peak load

1. Introduction

Electricity consumption has rapidly increased globally over the last few decades. The ever-growing electricity loads have affected the stability of electricity grids. If the demand exceeds the capacity reserved by power generators in the grid, critical failures such as overloads of power transmitters or blackouts may happen. Hence, it is important to manage a power load so that it can be controlled against the retained capacity of the grid (Fischetti et al., 2015). Especially in South Korea, the daily peak load has shown a relatively higher growth rate than the average power load over the course of

*Corresponding author

a day (Ministry of Trade Industry and Energy (MOTIE), 2017). This trend indicates that the peak load is getting closer to the retained capacity and that the load profiles fluctuate significantly.

A simple solution is to increase the number of generating resources. However, as sustainability is being avidly pursued by policymakers, interest in expanding renewable energy sources (RESs) that alleviate environmental issues, rather than in establishing conventional large-scale power plants, is rising (Azimian et al., 2022). As a result, many Organisation for Economic Co-operation and Development (OECD) countries have made efforts to invest in RESs and have retained a number of RESs. However, due to the dynamics of the intermittent RES-based generation, a high energy penetration has not been achieved, despite the sufficient capacity of RESs (Rana et al., 2020). In addition, the vast number of secured RESs have affected the generation of existing energy sources and have resulted in curtailment. Specifically, in California's grid system, the "duck curve" was monitored, in which the timing imbalance between peak load and RES-based generation is getting worse (Calero et al., 2022). To overcome these problems, the notion of the microgrid is being considered as an alternative. Microgrids are energy systems that contain RESs such as photovoltaics (PVs) and wind turbines (WTs) and dispatchable resources such as micro-gas turbines (MTs) and fuel cells (FCs), which can operate independently in a decentralized manner. The community microgrid (CMG) is a type of microgrid established for serving a particular community of residential loads. CMG can operate in an isolated environment to satisfy its connected loads and can also exchange power by being connected to the main grid (Cornélusse et al., 2019; Bidram et al., 2020). Unlike the conventional grid, CMG possesses the capability of a bidirectional flow of energy/information. This property enables CMGs to facilitate the integration of a high amount of residential energy. Furthermore, it also allows end-users (consumers) to produce energy using distributed generators (DGs) such as RESs and dispatchable resources. The dispatchable resources, including MTs using existing fossil fuels and FCs operated by hydrogen, allow the CMGs to compensate for the uncertainty of RES-based generation. In doing so, it turns the passive consumers into "prosumers" (consumer + producer). These prosumers can sell the surplus energy to the main grid or their neighbors by participating in the electricity market (Wu et al., 2016). As a result, they can save on their electricity bills or make financial gains.

Through the bidirectional flow of energy/information between the grid operator and end-users, the grids can also adapt more readily to increased penetration of RESs and encourage users' participation in energy savings and cooperation through a demand response (DR) program. DR program aims to manage demanded loads to match the retained energy resources without adding new generation capacity (Haider et al., 2016). An important issue in smart grids is how to design a DR program to reduce peak load and to better utilize DGs in microgrids (Borges et al., 2020).

There are many studies addressing DR programs in the scheduling of microgrids using bilevel programming approaches. Jalali et al. (2017) investigated the decision-making strategy of a distribution network operator considering multiple microgrid systems that seek to maximize their profits. In the integrated system, the microgrids can save electricity bills by shifting their loads from high market price hours to low market price hours. Van Ackooij et al. (2018) investigated a contract proposition problem to evaluate to what extent the main grid can supply microgrids without violating production constraints. Tao et al. (2020) addressed a bilevel optimization problem in which a power provider and multiple microgrids are considered. They focused on designing a real-time pricing program to maximize the provider's profit, which corresponded to the microgrids' response to the program. Rasheed et al. (2020) presented a real-time pricing mechanism that calculates

electric vehicle charging prices with the objective of cost reduction and power system stability. Li et al. (2018) investigated an optimal scheduling time frame of an isolated microgrid with an electric vehicle battery swapping station, and they did so taking into account multi-stakeholder scenarios. Quashie et al. (2018) proposed a bilevel program to minimize the planning and operational costs of microgrids, while the lower-level problem represented a grid system operator (GSO) whose primary duty was to ensure a reliable power supply. Nikzad and Samimi (2021) introduced a bilevel stochastic programming model for a central controller and microgrids, considering an incentive-based DR and real-time pricing. Kostarelou and Kozanidis (2021) considered the problem of devising an optimal price-bidding setup for a provider. They proposed a bilevel optimization model for maximizing the provider's profit in response to the minimization of the total bid costs of decentralized system operators.

To the best of our knowledge, the existing bilevel programming approaches that consider DR programs, such as real-time pricing and price-bidding, as described in Kostarelou and Kozanidis (2021), Nikzad and Samimi (2021) and Tao et al. (2020), were only focused on operations in a microgrid. As a result, the microgrid's operation, which may affect other generating sources belonging to the main grid, has not been restricted. In addition, even if a DR program that can realize a peak load reduction was designed, it would be limited in providing enough motivation for end-users to form a decentralized grid system.

This paper focuses on investigating the above-mentioned issues, and the contributions of this study are summarized as follows.

1. A way to investigate the system-side benefits, such as peak load reduction, a system model with a system operator, and a microgrid, is proposed based on a bilevel structure. In the system model, one decision-maker among two is entitled to design a subsidy strategy as a DR program. The other one seeks to find the optimal configuration of the microgrid and the optimal power schedule to its total relevant cost, including the capital costs of new system devices such as DGs and an energy storage system (ESS). As a result, the trade-off between the peak load reduction and the budget used for the DR program was carefully addressed.
2. Although the problem structure is related to the Stackelberg leader–follower game, the problem does not allow a sequential solution process of solving the Stackelberg model by exploring the follower's best response to the leader's decision-making due to the violation of the follower's decision variables on the leader's constraints. Hence, to solve the bilevel optimization problem, an efficient algorithm was devised based on two reformulation and decomposition approaches. The proposed algorithm guarantees that the bilevel solution can be obtained for practical instances within a reasonable time.
3. Through computational experiments, a set of microgrid configurations was evaluated and compared with the subsidy strategies of the GSO. In addition, a sensitivity analysis that examines the change in peak load was conducted.

The remainder of the paper is organized as follows. Section 2 describes the implemented system model of the GSO and CMG, as well as the mathematical model considering both decision makers. Section 3 presents a proposed solution strategy. Section 4 offers and discusses the simulation results, verifying the validity of the proposed system model. Finally, conclusions are drawn and areas for future work are recommended in Section 5.

2. System model and problem formulation

2.1. Problem statement

The implemented system model consists of the GSO, responsible for the secure operation and control of the grid network, and the CMG, which manages its DGs and residential loads. The system model of the GSO and the CMG is presented in Fig. 1. In the model, the GSO seeks to find an appropriate strategy to reduce the peak load of the upcoming CMG. As a strategy, the GSO can fund the installation of DGs to the CMG by subsidizing a portion of the DG's capital cost. Once the GSO determines a subsidy rate for a DG, the CMG can save on the cost of installing the DG according to the rate in composing the upcoming microgrid. Meanwhile, the total subsidy to the CMG is restricted to the budget set by the GSO. In the model, it is noted that the peak load is measured as the maximum power that the CMG exchanges with the main grid. The planning horizon of the CMG scheduling is set on a daily basis assuming demand remains unchanged for long-term planning periods.

The CMG looks for the optimal configuration of the microgrid with DGs to save on the total relevant cost. The DG units considered in the configuration include an MT, an FC, PVs, a WT, and an ESS. In particular, the MT and the FC are considered dispatchable sources, and they can produce power by consuming the required resources. Meanwhile, PVs and the WT are considered undispatchable sources, and they can generate power based on the corresponding energy potential due to their intermittent nature (Tsui and Chan, 2012). In this study, the uncertainty of solar radiation and wind speed have not been considered to avoid the complexity. The CMG with DGs is connected to the main grid and can participate in the bidirectional power exchange when required. The power exchange depends on the power schedule of the CMG and the electricity price from the main grid. The power schedule includes the output power of DGs, the charging/discharging power of the ESS, and the demand loads of a microgrid. Each DG can generate power when the DG is installed in the microgrid system. Similarly, charging/discharging power is available when the ESS is included in the system. In the system model, there are two types of demand loads in the CMG. The first type of loads corresponds to load demand from daily use such as residential and commercial loads. The residential and commercial loads are from day-ahead hourly predicted data. The second type of loads is related to power loads in charging electric vehicles and measured based on each charging schedule with a rated charging power.

2.2. Problem formulations

In the system model, the GSO is faced with the problem of minimizing the peak load of the CMG, subjected to the restriction that the CMG's total relevant cost is minimized (i.e., a bilevel optimization problem). Specifically, the major decision set by the GSO (i.e., subsidy rates for DGs) affects the best design of the microgrid and the power schedule on the CMG. Those decisions of the CMG consequently define the load profile and peak load that the CMG is interested in. Hence, the addressed problem is formulated based on a bilevel program in which the GSO and the CMG are considered as leader and follower, respectively. Let $\mathbb{x}^L$, $\mathbb{x}^F$, and $\mathbb{y}^F$ denote the continuous variables

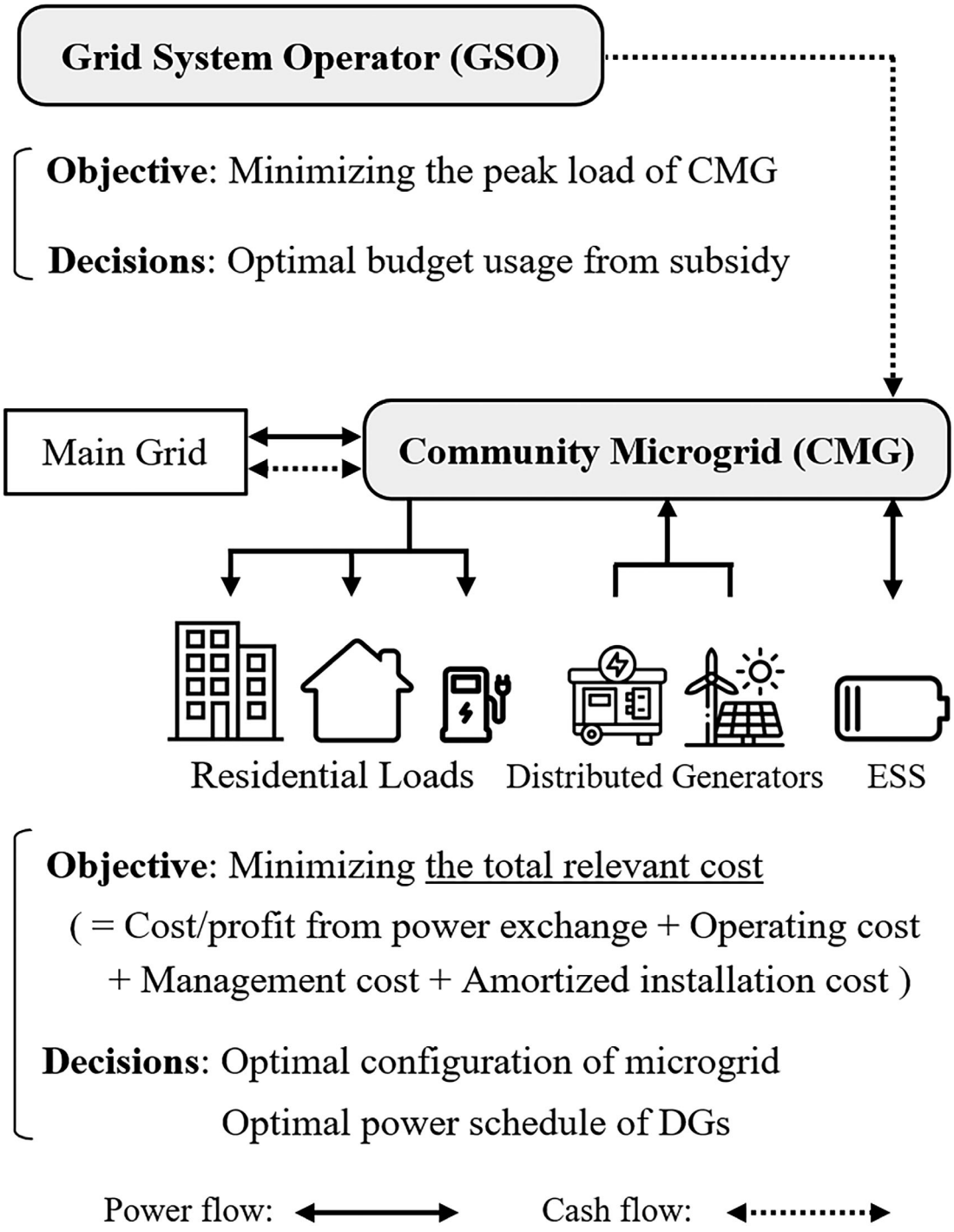

Fig. 1. Problem statement of the grid system operator (GSO) and the community microgrid (CMG). DGs, distributed generators; ESS, energy storage system.

of the leader, the continuous variables of the follower, and the discrete variables of the follower, respectively. The decision variables for the bilevel optimization problem can be represented as (1)–(3).

$$\mathbb{x}^L = [x_i \; x_{ESS}], \tag{1}$$

$$\mathbb{x}^F = \left[p_t \; p_{lt} \; p_t^{\text{cha}} \; p_t^{\text{dis}} \; p_{it}^{\text{gen}} \; p_t^{\text{in}} \; p_t^{\text{out}}\right], \tag{2}$$

$$\mathbb{y}^F = [y_i \; y_{ESS} \; \lambda_{la}], \tag{3}$$

where x_i and x_{ESS} in the leader's continuous variables are the subsidy rates for DGs and the ESS, respectively; p_t, p_{lt}, p_t^{cha}, p_t^{dis}, p_{it}^{gen}, p_t^{in}, and p_t^{out} in the follower's continuous variables represent the total power demand of the CMG, the power demand of loads, the charging/discharging power of the ESS, the output power of DGs, and the inbound/outbound power of the CMG, respectively; y_i, y_{ESS}, and λ_{la} in the follower's discrete variables are the binary variables indicating the selection of DGs, the ESS, and the schedule of a load when they are equal to one, respectively. It should be noted that i represents a DG, t is a time slot, l indicates a demand load, and s is related to an ordinal index of alternatives on possible schedules. Using the standard mathematical form, the addressed bilevel optimization problem can be described as follows:

$$\min_{\mathbb{x}^L} F\left(\mathbb{x}^L, \mathbb{x}^F, \mathbb{y}^F\right); \tag{4}$$

$$\text{s.t. } G_i\left(\mathbb{x}^L, \mathbb{x}^F, \mathbb{y}^F\right) \leq 0, \; i = 1, \ldots, \; p; \tag{5}$$

$$H_i\left(\mathbb{x}^L, \mathbb{x}^F, \mathbb{y}^F\right) = 0, \; i = 1, \ldots, \; q \tag{6}$$

$$\mathbb{x}^L \in \mathbb{R}^n \tag{7}$$

$$\text{where } \left(\mathbb{x}^F, \mathbb{y}^F\right) \in \arg\min_{\mathbb{x}^F, \mathbb{y}^F} f\left(\mathbb{x}^L, \mathbb{x}^F, \mathbb{y}^F\right) \tag{8}$$

$$\text{s.t. } g_i\left(\mathbb{x}^L, \mathbb{x}^F, \mathbb{y}^F\right) \leq 0, \; i = 1, \ldots, \; p'; \tag{9}$$

$$h_i\left(\mathbb{x}^L, \mathbb{x}^F, \mathbb{y}^F\right) = 0, \; i = 1, \ldots, \; q' \tag{10}$$

$$\mathbb{x}^F \in \mathbb{R}^{n'}, \mathbb{y}^F \in \mathbb{B}^{m'} \tag{11}$$

where F is the leader's objective function. G_i and H_i are inequality and equality constraints in the leader's problem, respectively. Similarly, f, g_i, and h_i are the objective function, inequality, and equality constraints in the follower's problem, respectively.

The following subsections introduce the leader's problem in (4)–(7) and the follower's problem in (8)–(11).

2.2.1. Leader's problem

The objective of the leader (i.e., the GSO) in the bilevel optimization problem is to minimize the peak load of the CMG over the planning period. In the model, the planning period is considered

as a day. Let T denote the set of time slots. The objective function of the GSO can be formulated as (12).

$$\min_{\mathbb{x}^L, \mathbb{x}^F, \mathbb{y}^F} F\left(\mathbb{x}^L, \mathbb{x}^F, \mathbb{y}^F\right) = \min \max_t \left\{ p_t^{\text{in}} - p_t^{\text{out}} \right\}. \tag{12}$$

Denote DGs as $I = \{\text{MT, FC, PV, WT}\}$. We note that a grid-connected device for electricity storage (i.e., ESS) is not included in I. The major decision variables on subsidy rates are defined in (13).

$$\text{s.t. } 0 \le x_i \le 1, \ \forall i \in I \text{ and } 0 \le x_{ESS} \le 1. \tag{13}$$

The subsidies on DGs and the ESS are supported based on the subsidy rates when the follower decides to install the corresponding devices into the microgrid. The total subsidy is available within the budget of the GSO, B, as shown in (14). We note that the following budget constraint can be moved to the follower's problem because the addressed model only considers a single follower in this study, and the constraint corresponds to the single follower.

$$\sum_i \alpha_i^{CRF} \pi_i x_i y_i + \alpha_{ESS}^{CRF} \pi_{ESS} x_{ESS} y_{ESS} \le B, \tag{14}$$

where α_i^{CRF} and α_{ESS}^{CRF} are capital recovery factors of DGs and the ESS, respectively; π_i and π_{ESS} denote capital costs of DGs and the ESS, respectively.

2.2.2. Follower's problem

The objective of CMG is to minimize the total relevant cost over the planning period. The total relevant cost includes the operating/maintenance costs of DGs and the ESS and the total capital costs of DGs. For operating/maintenance costs, we assumed that each cost function is linear, no start-up or shut-down cost is considered, and no minimum online or offline time for the generators is allowed. The capital cost of a DG unit is calculated by amortizing the installation cost of the unit as described in (15).

$$\begin{aligned} &\min \sum_t \left[c_t^{\text{buy}} p_t^{\text{in}} - c_t^{\text{sell}} p_t^{\text{out}} + \sum_i \left(c_i^{\text{oper}} / \alpha_i^{\text{gen}} + c_i^{\text{main}} \right) p_{it}^{\text{gen}} + c_{ESS}^{\text{main}} \left(p_t^{\text{cha}} + p_t^{\text{dis}} \right) \right] \\ &+ \sum_i \alpha_i^{CRF} \pi_i \left(1 - x_i\right) y_i + \alpha_{ESS}^{CRF} \pi_{ESS} \left(1 - x_{ESS}\right) y_{ESS}, \end{aligned} \tag{15}$$

where c_t^{buy} and c_t^{sell} are per unit cost of electricity buying and selling, respectively. The operating cost, maintenance cost, and generation efficiency of a DG are denoted by c_i^{oper}, c_i^{main}, and α_i^{gen}, respectively. c_{ESS}^{main} represents the maintenance cost of the ESS.

The active power of dispatchable sources such as the MT and the FC is available when the corresponding device is installed to the microgrid and is limited by their upper and lower limits, $\underline{P_i}$ and $\bar{P}_i$. Similarly, the active power of undispatchable sources such as PVs and the WT can be generated based on the predicted energy potential P_i^{RES} even if the device is connected to the microgrid.

Meanwhile, the ramp rate of power is restricted by the ramp-down rate and the ramp-up rate, $\Delta \underline{P_i}$ and $\Delta \bar{P}_i$. The constraints for DGs are presented below in (16)–(18).

$$\underline{P_i} y_i \le p_{it}^{\text{gen}} \le \bar{P}_i y_i, \ \forall i \in I \backslash I_{RES}, \ \forall t, \tag{16}$$

$$p_{it}^{\text{gen}} \le P_i^{RES} y_i, \ \forall i \in I_{RES}, \ \forall t, \tag{17}$$

$$\Delta \underline{P_i} y_i \le p_{it}^{\text{gen}} - p_{i,t-1}^{\text{gen}} \le \Delta \bar{P}_i y_i, \ \forall i \in I, \ \forall t, \tag{18}$$

where I_{RES} denotes the set of undispatchable sources.

The charging and discharging rates of the ESS are limited by the maximum charging and discharging rates, respectively. The energy level in the ESS at time, t, should be larger than the minimum capacity of the ESS, $\underline{E}$, and lower than the maximum capacity of the ESS, $\bar{E}$. The constraints for the ESS are described in (19)–(21).

$$0 \le p_t^{\text{cha}} \le \bar{P}^{\text{cha}} y_{ESS}, \ \forall t \tag{19}$$

$$0 \le p_t^{\text{dis}} \le \bar{P}^{\text{dis}} y_{ESS}, \ \forall t \tag{20}$$

$$\underline{E} y_{ESS} \le \sum_{i=1}^{t} \left(\alpha^{\text{cha}} p_i^{\text{cha}} - p_i^{\text{dis}} / \alpha^{\text{dis}} \right) \le \bar{E} y_{ESS}, \ \forall t \tag{21}$$

where α^{cha} and α^{dis} are charging and discharging the efficiency of the ESS, respectively.

The total power demand of the CMG, p_t, is the sum of all loads at time, t, as presented in (22). In the system model, the two types of demand loads are denoted by L_1 and L_2. In the model, the loads in the first type are assumed to be predicted in advance and are constant (Moghaddam et al., 2011). The loads in the second type are controllable by the CMG. For load $l \in L_1$, its power demand at t is set by the constant load profile $\tilde{p}_{lt}$ as shown in (23). For load $l \in L_2$, its power demand at t is set by the load profile E_{lat} defined by schedule a when the schedule is accepted. It should be noted that a schedule represents the independent operation plan associated with load $l \in L_2$. For each operation plan, only one start time is allowed and the schedule operates consecutively once it starts. Specifically, the load profile E_{lst} associated with load $l \in L_2$ and schedule s is defined by rated power E_a^{o}, and the time when the rated power is initially demanded, $\underline{T_{la}}$ for $t \in [\underline{T_{la}}, \underline{T_{la}} + len_l - 1]$ where len_l denotes the duration of power usage. Meanwhile, the load profile E_{lat} at the other times requires the minimum rated power E_l^{o}. The load profile for load $l \in L_2$ is set by one of several alternative schedules as presented in (24)–(26).

$$p_t = \sum_l p_{lt}, \forall t \tag{22}$$

$$p_{lt} = \tilde{p}_{lt} \ , \ \forall l \in L_1, \ \forall t \tag{23}$$

$$\sum_a E_{lat} \lambda_{la} = p_{lt} \ , \ \forall l \in L_2, \forall t \in \left[\underline{T_l}, \bar{T}_l \right] \tag{24}$$

$$E_{lat} := \begin{cases} E_l, \ t \in [\underline{T_{la}}, \underline{T_{la}} + len_l - 1] \\ E_l^{\mathrm{o}}, \ \text{otherwise} \end{cases}, \ \forall a, \ \forall l \in L_2; \tag{25}$$

$$\sum_a \lambda_{la} = 1, \ \forall l \in L_2. \tag{26}$$

Constraints in (27) show the power balance equation.

$$p_t^{\mathrm{in}} - p_t^{\mathrm{out}} + \sum_i p_{it}^{\mathrm{gen}} = p_t + \alpha^{\mathrm{cha}} p_t^{\mathrm{cha}} - \alpha^{\mathrm{dis}} p_t^{\mathrm{dis}}, \ \forall t. \tag{27}$$

All the continuous decision variables of followers, such as p_t, p_{lt}, p_t^{cha}, p_t^{dis}, p_{it}^{gen}, p_t^{in}, and p_t^{out}, are set to non-negative as defined in (11). Meanwhile, some solutions of the follower's problem might not be feasible for the leader's problem, even if the decision variables satisfy the constraints in (16)–(27). Specifically, this is because the decision variables might violate the leader's constraints, such as (14). This characteristic of the problem does not allow backward induction, a sequential solution process of solving the Stackelberg leader–follower model by exploring the follower's best response to the leader's decision-making (Basdere et al., 2013; Bianco et al., 2015; Noh et al., 2019). Therefore, to obtain a feasible solution, we employ a bilevel programming approach, namely, transforming a bilevel program into an equivalent single-level optimization problem (Kovács and Kovács, 2019). This reformulation technique cannot be applied to the introduced bilevel program directly because the technique is based on Karush–Kuhn–Tucker (KKT) conditions and the follower's problem contains discrete decision variables (Zeng and An, 2014; Yue et al., 2019). In the next section, we settle this by decomposing the bilevel program into a master problem (MP) and subproblems, and we introduce a reformulation-and-decomposition algorithm.

3. Reformulation-and-decomposition algorithm

In this section, we will first reformulate the proposed bilevel program in (4)–(11) into an equivalent single-level mathematical program in which the follower's program in (8)–(11) is extended based on all the combinations of discrete variables. The reformulated program could be computationally intractable because the extended formulation has as many additional constraints and variables as the number of all combinations. To handle this characteristic, we introduce an MP and subproblems, which substitute for the reformulated program, and then we apply a decomposition approach to efficiently solve the problem.

3.1. Reformulation

The proposed bilevel program is reformulated through optimal value reformulation (Chen et al., 1995). Specifically, if all the binary variables are fixed as constants, the follower's program transforms into a continuous convex program, equivalently substitutable by the corresponding KKT conditions (Yue and You, 2017). Hence, we can replace the follower's program with KKT

conditions associated with combinations of discrete variables. If we enumerate KKT conditions corresponding to all possible combinations of discrete variables, the set of KKT conditions guarantees the optimality of the follower's problem in the extended formulation. The entire single-level program, which is equivalent to the bilevel program, is as follows:

$$\min_{\mathbb{x}^L} F\left(\mathbb{x}^L, \mathbb{x}_0^F, \mathbb{y}_0^F\right); \tag{28}$$

$$\text{s.t.} G_i\left(\mathbb{x}^L, \mathbb{x}_0^F, \mathbb{y}_0^F\right) \leq 0,\ i = 1, \ldots,\ p; \tag{29}$$

$$H_i\ \left(\mathbb{x}^L, \mathbb{x}_0^F, \mathbb{y}_0^F\right) = 0,\ i = 1, \ldots,\ q \tag{30}$$

$$g_i\left(\mathbb{x}^L, \mathbb{x}_0^F, \mathbb{y}_0^F\right) \leq 0,\ i = 1, \ldots,\ p' \tag{31}$$

$$h_i\ \left(\mathbb{x}^L, \mathbb{x}_0^F, \mathbb{y}_0^F\right) = 0,\ i = 1, \ldots,\ q' \tag{32}$$

$$\frac{\partial f}{\partial \mathbb{x}_s^F} + \sum_{i=1}^{p'} u_{is} \frac{\partial g_i}{\partial \mathbb{x}_s^F} + \sum_{i=1}^{q'} v_{is} \frac{\partial h_i}{\partial \mathbb{x}_s^F} = 0, \forall s \in S; \tag{33}$$

$$g_i\left(\mathbb{x}^L, \mathbb{x}_s^F, \mathbb{y}_s^F\right) \leq 0,\ i = 1, \ldots,\ p'; \forall s \in S; \tag{34}$$

$$h_i\ \left(\mathbb{x}^L, \mathbb{x}_s^F, \mathbb{y}_s^F\right) = 0,\ i = 1, \ldots,\ q'; \forall s \in S \tag{35}$$

$$u_{is} \cdot g_i\ \left(\mathbb{x}^L, \mathbb{x}_s^F, \mathbb{y}_s^F\right) = 0,\ i = 1, \ldots,\ p'; \forall s \in S; \tag{36}$$

$$u_{is} \geq 0,\ i = 1, \ldots,\ p'; \forall s \in S \tag{37}$$

$$f\left(\mathbb{x}^L, \mathbb{x}_0^F, \mathbb{y}_0^F\right) \leq f\left(\mathbb{x}^L, \mathbb{x}_s^F, \mathbb{y}_s^F\right), \forall s \in S \tag{38}$$

$$\mathbb{x}_s^F \in \mathbb{R}_+^{n'}, \forall s \in S \tag{39}$$

$$\mathbb{x}^L \in \mathbb{R}^n,\ \mathbb{x}_0^F \in \mathbb{R}_+^{n'},\ \mathbb{y}_0^F \in \mathbb{B}^{m'} \tag{40}$$

where $\mathbb{x}_0^F$ and $\mathbb{y}_0^F$ are the follower's auxiliary decision variables in (4)–(11). $\mathbb{x}_s^F$ and $\mathbb{y}_s^F$ denote the follower's continuous variables and fixed binary variables corresponding to combination s, respectively. S is the set of all combinations of the follower's binary variables. In the single-level program, all the auxiliary variables are constrained in the same way as in (5) and (6) and (9) and (10), as described in (29)–(32). Constraints in (33)–(38) are established by replacing the follower's program with a set of KKT conditions equivalent to any combinations of fixed binary variables. For combination s, the KKT conditions on the follower's program are presented in (33)–(38). The stationary, primal feasibility, complementary slackness, and dual feasibility constraints are in (33)–(37), respectively. Here, u_{is} and v_{is} denote the dual variables of the follower's program corresponding to combination s. The KKT conditions hold that the follower's continuous variables, $\mathbb{x}_s^F$, are optimal to the follower's program for any combinations of the follower's discrete variables. Consequently, $f(\mathbb{x}^L, \mathbb{x}_s^F, \mathbb{y}_s^F)$ in (38) would be the finite optimal value for combination s. Therefore, the auxiliary

variables $\mathbb{x}_0^F$ and $\mathbb{y}_0^F$ can be guaranteed to be the follower's optimal solution, which is enforced by (38).

However, the reformulated program contains bilinear terms that make it hard to take advantage of efficient optimization solvers based on branch-and-bound algorithms. Specifically, the subsidized capital costs of DGs and the ESS (i.e., $\pi_i x_i y_i$ and $\pi_{ESS} x_{ESS} y_{ESS}$) are included in (29) and (38). The complementary slackness constraints in (36) have bilinear terms in which the continuous variables $\mathbb{x}^L$ and $\mathbb{x}_s^F$ are multiplied by the related dual variables u_{is}. In the proposed algorithm, the complementary slackness constraints are replaced with two constraints by applying the big-M relaxation to remove the bilinear terms. The complementary slackness constraints can be replaced with the linear big-M constraints by introducing new auxiliary binary variables w_{is} for each complementary slackness constraint as shown in (41) and (42).

$$-g_i\left(\mathbb{x}^L, \mathbb{x}_s^F, \mathbb{y}_s^F\right) \leq M^P\left(1 - w_{is}\right),\ i = 1, \ldots,\ p'; \forall s \in S; \tag{41}$$

$$u_{is} \leq M^D w_{is},\ i = 1, \ldots,\ p'; \forall s \in S \tag{42}$$

where M^P and M^D are valid upper bounds for the primal and dual variables of the follower's problem, respectively. Finally, we have a mixed integer linear program (MILP) in (28)–(35) and in (37)–(42) with the fixed variables y_i and y_{ESS}, and the program is denoted by the MP. The extended program is equivalent to the bilevel program in (4)–(11) (see Appendix A). However, in the equivalent program, a number of combinations of the added auxiliary variables and the follower's binary variables possibly exist that cause intractability in solving the program. Therefore, we introduce iterative decomposition procedures that handle this issue in the next subsection.

3.2. Decomposition

The decomposition procedures make the solution process consider partial enumerations of possible combinations rather than accounting for all the combinations at once. In the proposed process, a restricted set of combinations (i.e., $S_0 \subset S$) is considered in each procedure. We substitute the restricted set S_0 for the complete set S in (34)–(38) of the MP. Consequently, a restricted MP (RMP) is obtained. It should be noted that the RMP is a relaxation of the MP since only a subset of the KKT constraints spans the solution space. Specifically, if we get an optimal solution of the RMP and its objective value, denoted as Θ^*, then the solution is in the relaxed solution space of the MP, and Θ^* provides a dual bound (or lower bound) to the MP. We note that the problem RMP provides a set of leader's optimal decisions, denoted as $\mathbb{x}^{L*}$, based on the restricted set iteratively.

Next, we introduce two subproblems, which are to find the follower's optimal objective value at a given leader's optimal decisions, $\mathbb{x}^{L*}$, and to check the bilevel feasibility. We denote the first subproblem as subproblem 1 (SP1), and the problem is in the form of (15)–(27) (i.e., the follower's problem), but with $\mathbb{x}^L$ fixed at $\mathbb{x}^{L*}$. The optimal objective value of SP1 is denoted as $\theta(\mathbb{x}^{L*})$. In SP1, there might be multiple optimal solutions, which calculate the same objective value, $\theta(\mathbb{x}^{L*})$. However, the multiple solutions may lead to a different leader's objective values despite the same objective value, $\theta(\mathbb{x}^{L*})$. Moreover, these solutions might not be satisfied with the leader's constraints. Here, the follower's solution that satisfies the leader's constraints and calculates the best leader's

objective value is denoted as an optimistic solution to the leader. The follower's solution that is invalid to the leader's constraints or that calculates the leader's worst objective value, we refer to it as subproblem 2 (SP2). Its purpose is to verify the existence of an optimistic solution for the follower and to confirm that the problem includes constraints (12)–(14), (16)–(27), and the following constraint (43).

$$f\left(\mathbb{x}^L, \mathbb{x}^F, \mathbb{y}^F\right) \leq \theta\left(\mathbb{x}^{L*}\right). \tag{43}$$

SP2 aims to find a bilevel solution at a specified $\mathbb{x}^{L*}$, where the goal is to minimize the leader's objective function while regulating the follower's objective function through $\theta(\mathbb{x}^{L*})$. Successfully solving SP2 leads to a solution that meets bilevel feasibility criteria. This means that the optimal decisions of the follower in SP2 determine the optimal objective value, $\theta(\mathbb{x}^{L*})$, derived from SP1. Similarly, the leader's optimal decisions within the SP2 aim to minimize their objective value optimistically. The optimal value achieved in SP2 is represented as $\Theta_0(\mathbb{x}^{L*})$, setting a primal or upper bound for the bilevel problem. A divergence between the primal and dual bounds suggests the need for a more constrained solution space in the RMP. To obtain non-increasing primal bounds, a KKT-condition-based feasibility constraints (KC) in (33)–(38) is added to the RMP at each step. This KC reflects a specific set of the follower's binary choices. During decomposition, the next KC is formulated based on the current decisions of the follower, $\mathbb{y}_0^F$, retrieved from SP2. If SP2 yields a feasible bilevel solution, the subsequent KC is based on the binary choices from SP2. Within the RMP, the follower's decision variables, denoted by $\mathbb{x}_{k+1}^F$ and $\mathbb{y}_{k+1}^F$, are determined by the current decisions, $\mathbb{y}_0^F$, and are bound by the related KC in (33)–(38), considering the current iteration k. Conversely, if SP2 fails to find feasible solutions, the upcoming KC is created according to the follower's binary decisions from SP1.

3.3. Reformulation-and-decomposition algorithm

Based on the RMP and two subproblems, SP1 and SP2, we introduce a flowchart of the reformulation-and-decomposition algorithm as illustrated in Fig. 2. In solving the RMP, the bilinear terms incurred by the follower's binary variables such as $[y_i\ y_{ESS}]$ make it hard to take advantage of efficient optimization solvers. Hence, we simply partition the solution space to 2^n possible subspaces by enumerating any combinations of the binary variables on DG units where n is the number of DG units. If there are five binary variables for DGs, which consist of y_i and y_{ESS}, then the number of subspaces is equal to 2^5. The optimal solution of the current RMP is the best one among the solutions obtained from the subspaces. We noted that in searching each subspace, a powerful off-the-shelf optimization solver such as the CPLEX solver efficiently decides the solution state of the MILP. In other words, to obtain a candidate solution, the current RMP is not solved by searching all binary variables but rather performs multiple runs on the restricted set by the solver. This is to ensure optimality for the follower's problem whenever a combination is added to the restricted set. The restricted set of combinations only defines the binary variables for DGs (i.e., y_i and y_{ESS}, not λ_{la}). In running the decomposition procedure in the algorithm, the subset of the follower's binary decisions starts with $S_0 = \emptyset$ and expands by adding one element corresponding to $\mathbb{y}_{k+1}^F$ at the end of any given iteration k if the algorithm is not terminated.

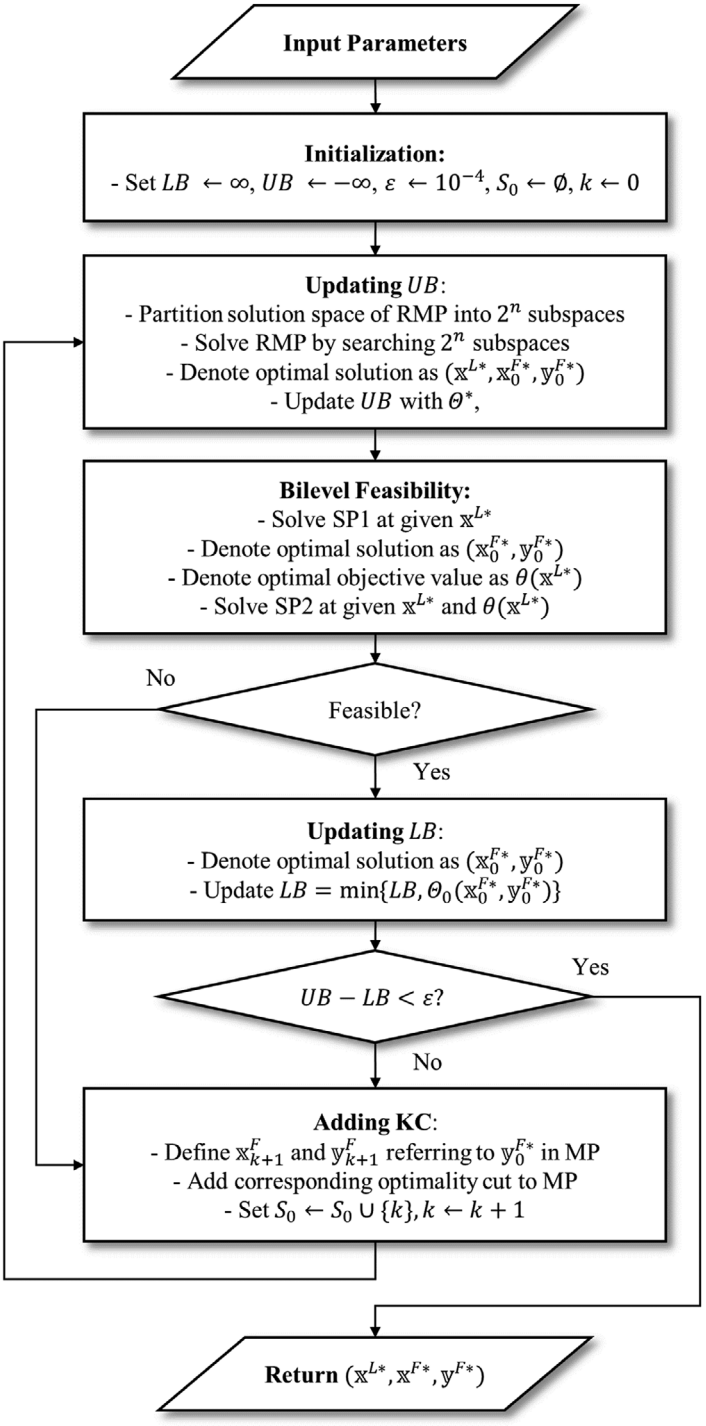

Fig. 2. Flowchart of the reformulation-and-decomposition algorithm. KC, KKT-condition-based feasibility constraints; MP, master problem; RMP, restricted master problem; SP1, subproblem 1; SP2, subproblem 2.

Table 1
Day-ahead hourly predicted data of community microgrid (CMG)

Time (hour)	PV (kW)	WT (kW)	Load (kW)	Price (¢/kWh)	Time (hour)	PV (kW)	WT (kW)	Load (kW)	Price (¢/kWh)
1	0	1.785	52	0.23	13	23.90	3.915	72	1.50
2	0	1.785	50	0.19	14	21.05	2.370	72	4.00
3	0	1.785	50	0.14	15	7.88	1.785	76	2.00
4	0	1.785	50	0.12	16	4.23	1.305	80	1.95
5	0	1.785	56	0.12	17	0.55	1.785	85	0.60
6	0	0.915	63	0.20	18	0	1.785	88	0.41
7	0	1.785	70	0.23	19	0	1.302	90	0.35
8	0.2	1.305	75	0.38	20	0	1.785	87	0.43
9	3.75	1.785	76	1.50	21	0	1.301	78	1.17
10	7.53	3.090	80	4.00	22	0	1.301	71	0.54
11	10.45	8.775	78	4.00	23	0	0.915	65	0.30
12	11.95	10.41	74	4.00	24	0	0.615	56	0.26

4. Computational experiments

To demonstrate the proposed system model and the developed reformulation-and-decomposition algorithm, we consider a case study on designing an upcoming microgrid as a pilot test. For the case study, we investigate the trade-off between the reduction of peak load and the budget used for the subsidies.

4.1. Experimental setting

In this study, configurations and operations of a microgrid for subsidy strategies were investigated to analyze the peak load reduction. There is a CMG with one constant power load in the first load type and three controllable power loads in the second load type. For the first load type, the day-ahead hourly predicted power load of the CMG is shown in Table 1 (Rana et al., 2020). For the second load type, there are three identical electric cars demanding power loads when charging the vehicles. The charging time of load $l \in L_2$ was given from 8 p.m. to 8 a.m., and the charging duration, l_l, was set as five hours. Consequently, eight possible schedules, in which charging starts from 8 p.m. to 3 a.m., are considered for each load in the second load type. The rated power of the load was set at 7 kWh, known as the power rating of the standard charger. The above parameters on the charging power load were identically applied to all the loads classified in the second load type. The CMG considers installing an MT, an FC, a WT, PVs, and an ESS on its microgrid and seeks to minimize the total relevant cost in operating the system. The parameters of the DG units and the ESS, which were scaled for adequate microgrid environments referring to Logenthiran et al. (2010), Moghaddam et al. (2011), Qi et al. (2018), and Sufyan et al. (2019), are presented in Table 2. For calculating the capital recovery factor, we set the interest rate as 6%. The lifetimes of DG units and the ESS are set as 10 years and three years, respectively. The round-trip efficiency is set to 90%. The initial state of charge of the ESS is assumed to be 60%. The budget of the GSO is set at

Table 2
Parameters of the distributed generator (DG) units and the energy storage system (ESS)

Device	Micro-gas turbine (MT)	Fuel cell (FC)	Photovoltaic (PV)	Wind turbine (WT)	ESS
Capital cost (M$/unit)	27	60	75	32.25	33
Min power (kW)	6	3	0	0	−30
Max power (kW)	30	30	25	15	30
Ramp-up rate (kW)	140	120	-	-	20
Ramp-down rate (kW)	–30	–60	-	-	−60
Operating cost (¢/kWh)	0.4	0.2	0	0	0
Maintenance cost (¢/kWh)	0.12	0.04	0.11	0.08	0.02

$50 as the baseline, and in the test to investigate the trade-off, the budget was changed from $0 to $100. We note that the budget is the capacity of the total amortized subsidies on DGs and the ESS. The ramping-up values of MT and FC are not limited by the corresponding production rates in the instances. This is because we are considering small-sized production units in this experimental setting.

All computational experiments are carried out on a PC with an Intel core i9-9900 Central Processing Unit (CPU) at 3.60 GHz and 32 GB RAM. All models and solution procedures were coded in C# using Concert Technology, which is from the CPLEX solver engine licensed by IBM ILOG. The version of the CPLEX solver engine used was 20.1, and the default setting of the solver engine was used to conduct the computational experiments. For the setting of the reformulation-and-decomposition algorithm, the tolerance ε for the developed algorithm is set to 10^{-4}. The upper bounds on primal and dual variables, M^P and M^D were set to 1000. The bound on the primal variable was calculated with the exact value of $\max\{\max_{\forall i}\{\bar{P}_i\}, \max_{\forall i}\{P_i^{RES}\}, \max_{\forall i}\{\nabla\bar{P}_i\}, \max_{\forall i}\{\bar{P}_i + \nabla\bar{P}_i\}, \bar{P}^{\text{cha}}, \bar{P}^{\text{dis}}, \bar{E},\}$. The bound of dual variables was obtained by running the trial-and-error procedure, the most commonly used technique in the literature, in the introduced experimental setting. It should be noted that we denote the solutions determined by the proposed algorithm as the best solutions rather than the optimal solutions because the upper bound obtained by the procedure may lead to suboptimal solutions for bilevel programs. Detailed descriptions and processes for setting the upper bounds are presented in Appendix B.

4.2. Performances of the proposed algorithm

In this chapter, we conducted computational experiments to evaluate the algorithm performance prior to the case study. First, we expected that the performance of the proposed algorithm would have a significant impact on integer variables. Therefore, to test the algorithm performance, computational experiments were performed by changing the maximum number of DG that can be installed in the microgrid from 1 to 3 for each type. In these experiments, the budget was set to 50.

The computational results are shown in Table 3. In the table, the instance number, maximum number of each DG, calculation time, and objective function are described. The maximum number was arbitrarily set, and the termination condition was set at 3600 seconds. As a result of the

Table 3
Performance test of the proposed algorithm varying the maximum number of DGs

Instance #	Maximum number of DGs					CPU time (seconds)	Peak load	Instance #	Maximum number of DGs					CPU time (seconds)	Peak load
	MT	FC	PV	WT	ESS				MT	FC	PV	WT	ESS		
1	1	1	1	1	1	7.2	21.11	32	3	2	2	2	2	2433.3	15.05
2	2	1	1	1	1	8.4	20.20	33	2	3	2	2	2	2926.2	15.05
3	1	2	1	1	1	8.7	19.20	34	2	2	3	2	2	3406.8	15.05
4	1	1	2	1	1	10.2	20.70	35	2	2	2	3	2	2047.6	15.05
5	1	1	1	2	1	7.8	21.05	36	2	2	2	2	3	3408.2	15.05
6	1	1	1	1	2	7.6	21.00	37	3	3	2	2	2	3546.8	15.05
7	2	2	1	1	1	12.8	19.70	38	3	2	3	2	2	2807.2	15.05
8	2	1	2	1	1	15.4	18.70	39	3	2	2	3	2	1866.3	14.11
9	2	1	1	2	1	13.2	18.76	40	3	2	2	2	3	3600+	N/A
10	2	1	1	1	2	15.8	19.73	41	2	3	3	2	2	907.2	14.09
11	1	2	2	1	1	73.2	19.11	42	2	3	2	3	2	2517.1	14.09
12	1	2	1	2	1	63.3	16.11	43	2	3	2	2	3	3116.8	14.09
13	1	2	1	1	2	45.5	19.09	44	2	2	3	3	2	1988.4	14.09
14	1	1	2	2	1	57.2	19.09	45	2	2	3	2	3	3506.8	14.95
15	1	1	2	1	2	77.1	19.09	46	2	2	2	3	3	1127.7	14.95
16	1	1	1	2	2	66.8	19.09	47	3	3	3	2	2	3600+	N/A
17	2	2	2	1	1	368.4	19.09	48	3	3	2	3	2	3600+	N/A
18	2	2	1	2	1	266.8	18.95	49	3	3	2	2	3	3600+	N/A
19	2	2	1	1	2	166.2	18.95	50	3	2	3	3	2	3600+	N/A
20	2	1	2	2	1	267.3	18.95	51	3	2	3	2	3	3600+	N/A
21	2	1	1	2	2	167.1	19.09	52	3	2	2	3	3	3600+	N/A
22	1	2	2	2	1	166.8	19.09	53	2	3	3	3	2	3600+	N/A
23	1	2	2	1	2	178.4	19.09	54	2	3	3	2	3	3600+	N/A
24	1	2	1	2	2	276.8	17.95	55	2	3	2	3	3	2847.2	14.95
25	1	1	2	2	2	166.2	17.95	56	2	2	3	3	3	3600+	N/A
26	2	2	2	2	1	2257.3	17.95	57	3	3	3	3	2	3600+	N/A
27	2	2	2	1	2	2266.6	17.95	58	3	3	3	2	3	3600+	N/A
28	2	2	1	2	2	2356.4	17.95	59	3	3	2	3	3	3600+	N/A
29	2	1	2	2	2	2256.1	17.09	60	3	2	3	3	3	3600+	N/A
30	1	2	2	2	2	3356.6	17.09	61	2	3	3	3	3	3600+	N/A
31	2	2	2	2	2	3506.2	17.09	62	3	3	3	3	3	3600+	N/A

experiments, when the total number of DG units was set to 12 or fewer, the algorithm completed the procedure and searched for the best solution within the time limit, except for the 40th instance. On the other hand, when it was set to 13 or more, the algorithm failed to complete the procedure and find the best solution within the time limit except for the 55th instance.

4.3. Results of the case study

In this case study, computational experiments were conducted based on the microgrid environments referred to by Logenthiran et al. (2010), Moghaddam et al. (2011), Qi et al. (2018), and Sufyan et al. (2019). To examine the trade-off between the peak load and the budget, we generated several

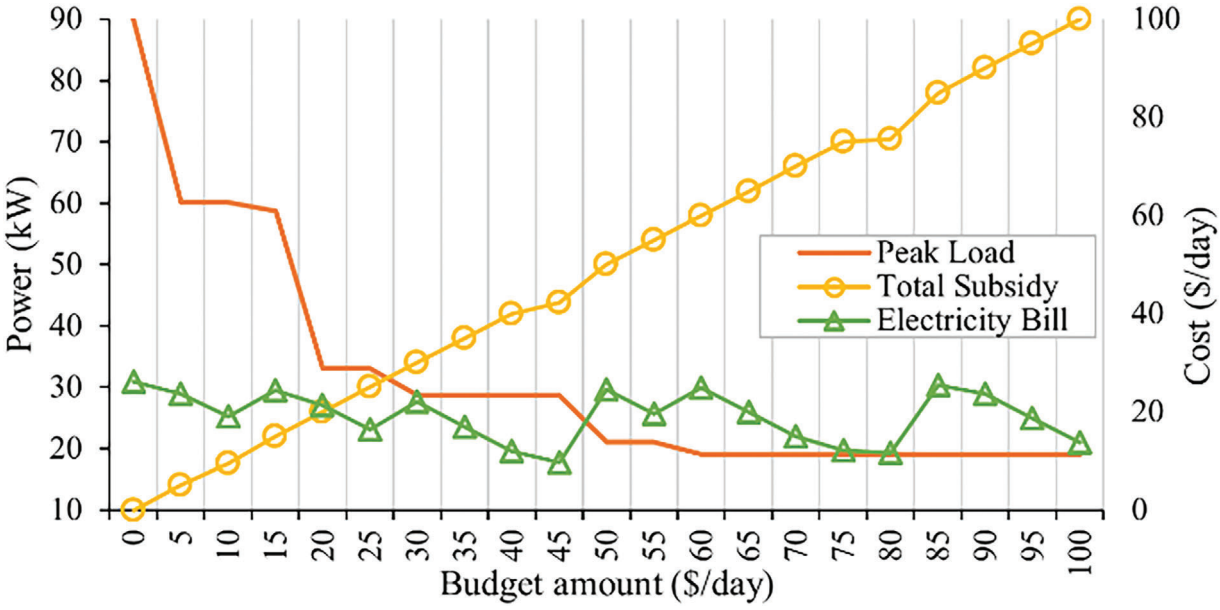

Fig. 3. The trade-off between the peak load and the budget.

problem instances by changing the budget for the subsidy strategy from 0 to 100. We solved the problem instances with the proposed reformulation-and-decomposition algorithm. The algorithm found the bilevel solutions of all the instances within 164 CPU seconds. The results of the subsidy strategies of the GSO that minimize the peak load and the best configuration of the CMG are presented in Table 3. In the table, the best subsidy rates for installing DGs and the ESS and the installed DGs and the ESS in a microgrid for each budget setting are given, as well as the optimal peak load of the CMG. We noted that the peak load is measured as the maximum power that the CMG exchanges with the main grid. As the budget increased, the results showed that the system model integrated microgrid-connected devices in order of MTs, FCs, WTs, the ESS, and PVs substantially and measured the non-increased peak load. Meanwhile, when the budget was set to \$15, WTs, of which the amortized capital cost is relatively cheaper than that of PVs, were alternatively considered to be installed due to the bilevel feasibility. In other words, the GSO set a subsidy rate for PVs instead of WTs because the budget was incapable of setting up an adequate subsidy rate to persuade the CMG to install a WT. Similarly, the results of setting the subsidy rate differently from the priority can be observed when the budget was set to \$50, \$55, and \$90. The trade-off between the budget and the peak load is illustrated in Fig. 3. In the figure, the solid orange line indicates the peak load of the CMG. The solid lines with a circle mark and a triangle mark represent the total subsidy and the follower's objective value, respectively. In the figure, the significant reduction in the peak load is illustrated. This result shows that the side effects of today's main grid from an expansion of RESs can be alleviated by attracting a decentralized grid (i.e., a microgrid). In addition, since the reduction of the peak load is obtained from the microgrid's decisions, which only focus on optimizing its individual benefit, it is shown to be an effective way to establish a subsidy rate to control the peak load.

Table 4
Results of subsidy rates of GSO and configuration of CMG

B	CPU time (seconds)	Peak load	Subsidy rates [y_i y_{ESS}]					Configuration [x_i x_{ESS}]				
			MT	FC	PV	WT	ESS	MT	FC	PV	WT	ESS
0	6.4	90.00										
5	6.1	60.20	0.52					1				
10	6.6	60.20	1					1				
15	6.2	58.70	0.37			1		1			1	
20	6.3	33.05	0.26	0.82				1	1			
25	6.2	33.05	1	0.72				1	1			
30	6.8	28.70	1	0.42		1		1	1		1	
35	7.6	28.70	1	0.66		1		1	1		1	
40	8.2	28.70	1	0.89		1		1	1		1	
45	6.8	28.70	1	1		1		1	1		1	
50	7.2	21.11	0.31	0.65			1	1	1			1
55	6.3	21.11	0.95	0.59			1	1	1			1
60	6.5	19.09	1	1		1	0.53	1	1		1	1
65	7.2	19.09	1	1		1	0.68	1	1		1	1
70	7.1	19.09	1	1		1	0.83	1	1		1	1
75	6.8	19.09	1	1		0.96	1	1	1		1	1
80	8.4	19.09	1	1		1	1	1	1		1	1
85	6.8	18.95	1	1	1	1	0.48	1	1	1	1	1
90	6.2	18.95	1	1	0.97		1	1	1	1	1	1
95	7.3	18.95	1	1	1	0.38	1	1	1	1	1	1
100	6.6	18.95	1	1	1	0.81	1	1	1	1	1	1

Abbreviation: GSO, grid system operator.

The best power schedules of the CMG related to the budgets of 25, 50, 75, and 100 are presented in Fig. 4a–d, respectively. The CMG's schedules are based on the best configuration of a microgrid. The corresponding configurations can be seen in Table 4. In the figure, the solid blue line indicates the total load, including the constant load in the first load type and the power loads in the second load type. The solid green line illustrates only the constant load. The active power of DGs and the ESS and the power that the CMG exchanges with the main grid are represented by stacked bars. We note that the surplus power exceeding the total load is used to charge the ESS unit as shown in Fig. 4b–d. The results show that during times of high power prices, the loads are satisfied by reducing power exchanges from the main grid and fully operating the installed DGs.

4.4. Sensitivity analysis

To investigate how changes in parameters affect both the peak load reduction and scheduling of the CMG, we carried out a sensitivity analysis by changing the min/max power of the ESS to –15/15 kW (small), –30/30 kW (medium), and –45/45 kW (large). Similarly, we used the generated instances in which the budget is changing from 0 to 100. The results can be found in Fig. 5. The results show that the Pareto frontier obtained for a large capacity of consumption dominates other

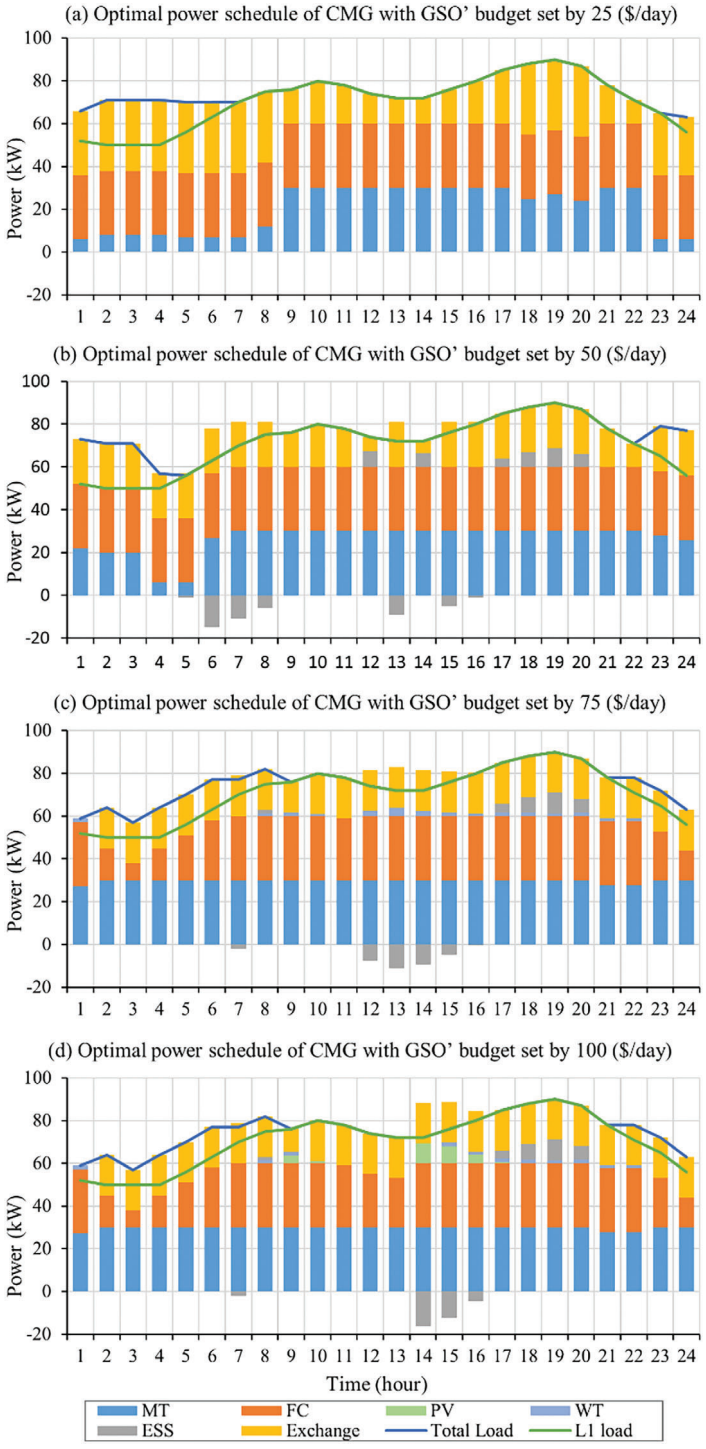

Fig. 4. The best operation schedule of system devices of the CMG.

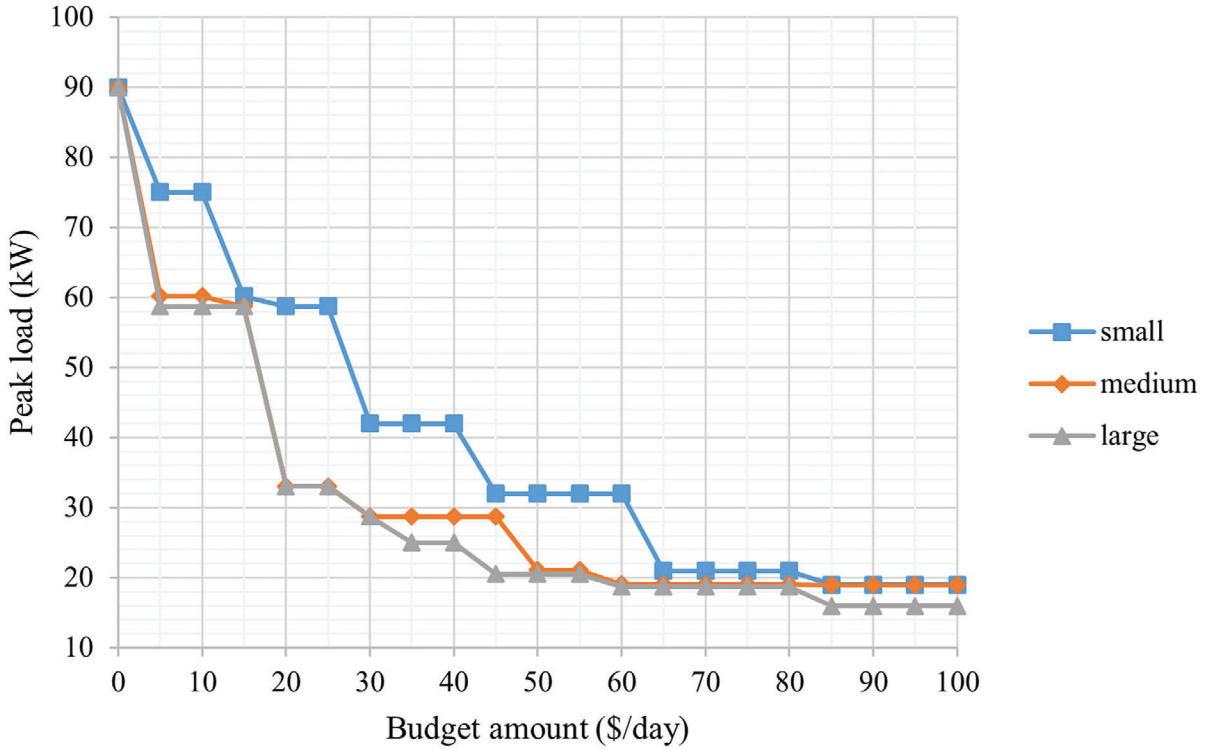

Fig. 5. Pareto frontiers with respect to the energy storage system capacity.

Pareto frontiers. This means that increasing the capacity of the ESS is effective in reducing peak demand.

5. Conclusion

We introduced a system model of a system operator and a microgrid based on the Stackelberg leader–follower model. In the system model, the leader is entitled to design a subsidy strategy as a DR program. Meanwhile, the follower seeks to find the optimal configuration of the microgrid and the optimal power schedule to its total relevant cost, including the capital costs of new system devices such as DGs and the ESS. We formulated the system model as a bilevel optimization problem. To find a bilevel solution of the problem, an efficient algorithm was devised based on two reformulation and decomposition approaches. Specifically, the follower's program was partitioned based on all the combinations of binary decisions and then replaced with the corresponding KKT conditions. Moreover, the existing linearities were adequately relaxed in the proposed solution procedures. The proposed reformulation-and-decomposition algorithm guaranteed that the bilevel solution could be obtained for the experimental instances in microgrid research within a reasonable time. We conducted computational experiments to test the efficiency of the algorithm's performance. The results showed that the maximum number of DGs affects the performance, and the algorithm failed to

complete the procedure within the limited time when the number of DG units was allowed to exceed 13 in total. Through computational experiments on a case study, the trade-off between the peak load reduction and the budget used for the DR program was carefully addressed. In addition, a set of microgrid configurations was evaluated and compared with the GSO's subsidy strategies. The sensitivity analysis reports managerial insights on designing a subsidy strategy with the relative capital cost of system devices such as DGs and the ESS. However, the limitations of this study exist as follows: a decision-making problem for a short time horizon is presented under the assumption of deterministic and unchanging demand, though the investments of DGs required long-term planning periods. The upper bound of dual variables, which affects algorithm calculation performance, was provided based on the empirical tuning process rather than the validity of the values. In addition, the size of the case study was limited, though we conducted it using instances reported in previous studies. Hence, setting up more practical instances is required for further research. For further directions on how to implement the addressed framework in practice, various types of DR programs, such as real-time pricing and other incentive programs, could be considered. In addition, uncertain factors such as demand, renewable generation, and electricity prices can be considered in further research.

Acknowledgments

The authors are grateful for the valuable comments from the area editor and three anonymous reviewers. This work was supported by the National Research Foundation of Korea (NRF) grants funded by the Korean government (Ministry of Science and ICT) [Grant Nos. RS-2023-00218913 and RS-2024-00337285].

References

Azimian, M., Amir, V., Mohseni, S., Brent, A.C., Bazmohammadi, N., Guerrero, J.M., 2022. Optimal investment planning of bankable multi-carrier microgrid networks. *Applied Energy* 328, 120121.

Basdere, M., Aras, N., Altinel, I.K., Afşar, S., 2013. A leader-follower game for the point coverage problem in wireless sensor networks. *European Journal of Industrial Engineering* 7, 635–656.

Bianco, L., Caramia, M., Giordani, S., Mari, R., 2015. Grid scheduling by bilevel programming: a heuristic approach. *European Journal of Industrial Engineering* 9, 101–125.

Bidram, A., Poudel, B., Damodaran, L., Fierro, R., Guerrero, J.M., 2020. Resilient and cybersecure distributed control of inverter-based islanded microgrids. *IEEE Transactions on Industrial Informatics* 16, 3881–3894.

Borges, Y.G.F., Schouery, R.C.S., Miyazawa, F.K., Granelli, F., da Fonseca, N.L.S., Melo, L.P., 2020. Smart energy pricing for demand-side management in renewable energy smart grids. *International Transactions in Operational Research* 27, 2760–2784.

Calero, I., Cañizares, C.A., Bhattacharya, K., Baldick, R., 2022. Duck-curve mitigation in power grids with high penetration of PV generation. *IEEE Transactions on Smart Grid* 13, 314–329.

Chen, Y., Florian, M., Floriant, M., 1995. The nonlinear bilevel programming problem:formulations,regularity and optimality conditions. *Optimization* 32, 193–209.

Cornélusse, B., Savelli, I., Paoletti, S., Giannitrapani, A., Vicino, A., 2019. A community microgrid architecture with an internal local market. *Applied Energy* 242, 547–560.

Fischetti, M., Sartor, G., Zanette, A., 2015. MIP-and-refine matheuristic for smart grid energy management. *International Transactions in Operational Research* 22, 49–59.

Haider, H.T., See, O.H., Elmenreich, W., 2016. A review of residential demand response of smart grid. *Renewable and Sustainable Energy Reviews* 59, 166–178.

Jalali, M., Zare, K., Seyedi, H., 2017. Strategic decision-making of distribution network operator with multi-microgrids considering demand response program. *Energy* 141, 1059–1071.

Jenabi, M., Ghomi, S.M.T.F., Smeers, Y., 2013. Bi-level game approaches for coordination of generation and transmission expansion planning within a market environment. *IEEE Transactions on Power Systems* 28, 2639–2650.

Kleinert, T., Labbé, M., Plein, F., Schmidt, M., 2020. There's no free lunch: on the hardness of choosing a correct big-M in bilevel optimization. *Operations Research* 68, 1716–1721.

Kostarelou, E., Kozanidis, G., 2021. Bilevel programming solution algorithms for optimal price-bidding of energy producers in multi-period day-ahead electricity markets with non-convexities. *Optimization and Engineering* 22, 449–484.

Kovács, A., Kovács, K., 2019. Bilevel programming approach to demand response management with day-ahead tariff. *Journal of Modern Power Systems and Clean Energy* 7, 1632–1643.

Li, Y., Yang, Z., Li, G., Mu, Y., Zhao, D., Chen, C., Shen, B., 2018. Optimal scheduling of isolated microgrid with an electric vehicle battery swapping station in multi-stakeholder scenarios: a bi-level programming approach via real-time pricing. *Applied Energy* 232, 54–68.

Logenthiran, T., Srinivasan, D., Khambadkone, A.M., Sundar Raj, T.S., 2010. Optimal sizing of an islanded microgrid using Evolutionary Strategy, 2010 IEEE 11th International Conference on Probabilistic Methods Applied to Power Systems, June 14–17, Singapore, pp. 12–17.

Ministry of Trade Industry and Energy (MOTIE), 2017. The 8th Basic Plan for Long-term Electricity Supply and Demand (BPLE) (2017-2031). Available at https://new.kpx.or.kr/menu.es?mid=a20407000000 (accessed 3 March 2023).

Moghaddam, A.A., Seifi, A., Niknam, T., Alizadeh Pahlavani, M.R., 2011. Multi-objective operation management of a renewable MG (micro-grid) with back-up micro-turbine/fuel cell/battery hybrid power source. *Energy* 36, 6490–6507.

Motto, A.L., Arroyo, J.M., Galiana, F.D., 2005. A mixed-integer LP procedure for the analysis of electric grid security under disruptive threat. *IEEE Transactions on Power Systems* 20, 1357–1365.

Nikzad, M., Samimi, A., 2021. Integration of designing price-based demand response models into a stochastic bi-level scheduling of multiple energy carrier microgrids considering energy storage systems. *Applied Energy* 282, 11 6163.

Noh, J., Kim, J.S., Sarkar, B., 2019. Two-echelon supply chain coordination with advertising-driven demand under Stackelberg game policy. *European Journal of Industrial Engineering* 13, 213–244.

Pineda, S., Morales, J.M., 2019. Solving linear bilevel problems using big-Ms: not all that glitters is gold. *IEEE Transactions on Power Systems* 34, 2469–2471.

Qi, J., Lai, C., Xu, B., Sun, Y., Leung, K.-S., 2018. Collaborative energy management optimization toward a green energy local area network. *IEEE Transactions on Industrial Informatics* 14, 5410–5418.

Quashie, M., Marnay, C., Bouffard, F., Joós, G., 2018. Optimal planning of microgrid power and operating reserve capacity. *Applied Energy* 210, 1229–1236.

Rana, J., Zaman, F., Ray, T., Member, S., Sarker, R., Juel Rana, M., 2020. Heuristic enhanced evolutionary algorithm for community microgrid scheduling. *IEEE Access* 8, 76500–76515.

Rasheed, M.B., Awais, M., Alquthami, T., Khan, I., 2020. An optimal scheduling and distributed pricing mechanism for multi-region electric vehicle charging in smart grid. *IEEE Access* 8, 40298–40312.

Sufyan, M., Abd Rahim, N., Tan, C., Muhammad, M.A., Sheikh Raihan, S.R., 2019. Optimal sizing and energy scheduling of isolated microgrid considering the battery lifetime degradation. *PLoS ONE* 14, 1–28.

Tao, L., Gao, Y., Liu, Y., Zhu, H., 2020. A rolling penalty function algorithm of real-time pricing for smart microgrids based on bilevel programming. *Engineering Optimization* 52, 1295–1312.

Tsui, K.M., Chan, S.C., 2012. Demand response optimization for smart home scheduling under real-time pricing. *IEEE Transactions on Smart Grid* 3, 1812–1821.

Van Ackooij, W., De Boeck, J., Detienne, B., Pan, S., Poss, M., 2018. Optimizing power generation in the presence of micro-grids. *European Journal of Operational Research* 271, 450–461.

Wu, L., Ortmeyer, T., Li, J., 2016. The community microgrid distribution system of the future. *Electricity Journal* 29, 16–21.

Yue, D., Gao, J., Zeng, B., You, F., 2019. A projection-based reformulation and decomposition algorithm for global optimization of a class of mixed integer bilevel linear programs. *Journal of Global Optimization* 73, 27–57.

Yue, D., You, F., 2017. Stackelberg-game-based modeling and optimization for supply chain design and operations: a mixed integer bilevel programming framework. *Computers & Chemical Engineering* 102, 81–95.

Zeng, B., An, Y., 2014. Solving bilevel mixed integer program by reformulations and decomposition. *Optimization* online. Available at https://optimization-online.org/wp-content/uploads/2014/07/4455.pdf (accessed 11 November 2022).

Zugno, M., Morales, J.M., Pinson, P., Madsen, H., 2013. Pool strategy of a price-maker wind power producer. *IEEE Transactions on Power Systems* 28, 3440–3450.

Appendix A

Reformulation of the extended bilevel program

The entire formulation of the single-level program obtained from reformulation is presented in (A1)–(A92). We noted that superscripts of variables, that is, $A7 - A28$, represent constraints in (A7)–(A28), respectively.

$$\min \max_{\forall t} \left\{ p_t^{\text{in}} - p_t^{\text{out}} \right\}, \tag{A1}$$

$$\text{s.t. } x_i \leq 1, \ \forall i \in I, \tag{A2}$$

$$x_{ESS} \leq 1, \tag{A3}$$

$$\sum_i \alpha_i^{CRF} \pi_i x_i y_{i,0} + \alpha_{ESS}^{CRF} \pi_{ESS} x_{ESS} y_{ESS,0} \leq B, \tag{A4}$$

$$x_i \geq 0, \ \forall i \in I, \tag{A5}$$

$$x_{ESS} \geq 0, \tag{A6}$$

$$\underline{P_i} y_{i,0} - p_{i,t,0}^{\text{gen}} \leq 0, \forall i \in I, \forall t, \tag{A7}$$

$$p_{i,t,0}^{\text{gen}} - \bar{P}_i y_{i,0} \leq 0, \ \forall i \in I, \ \forall t, \tag{A8}$$

$$p_{i,t,0}^{\text{gen}} - P_i^{RES} y_{i,0} \leq 0, \ \forall i \in I_{RES}, \ \forall t, \tag{A9}$$

$$p_{i,0,0}^{\text{gen}} - \Delta \bar{P}_i y_{i,0} \leq 0, \ \forall i \in I, \tag{A10}$$

$$\nabla \underline{P_i} y_{i,0} - p_{i,t,0}^{\text{gen}} + p_{i,t-1,0}^{\text{gen}} \leq 0, \ \forall i \in I, \ \forall t = 2, \ldots, 23, \tag{A11}$$

$$p_{i,t,0}^{\text{gen}} - p_{i,t-1,0}^{\text{gen}} - \Delta \bar{P}_i y_{i,0} \leq 0, \ \forall i \in I, \ \forall t = 2, \ldots, 23, \tag{A12}$$

$$p_{t,0}^{\text{cha}} - \bar{P}^{\text{cha}} y_{ESS,0} \leq 0, \ \forall t, \tag{A13}$$

$$p_{t,0}^{\text{dis}} - \bar{P}^{\text{dis}} y_{ESS,0} \leq 0, \ \forall t, \tag{A14}$$

$$\underline{\text{E}} y_{ESS,0} - \sum_{i=1}^{t} \left(\alpha^{\text{cha}} p_{i,0}^{\text{cha}} - p_{i,0}^{\text{dis}} / \alpha^{\text{dis}} \right) \leq 0, \forall t, \tag{A15}$$

$$\sum_{i=1}^{t} \left(\alpha^{\text{cha}} p_{i,0}^{\text{cha}} - p_{i,0}^{\text{dis}} / \alpha^{\text{dis}} \right) - \bar{E} y_{ESS,0} \leq 0, \forall t, \tag{A16}$$

$$p_{t,0} - \sum_{l} p_{l,t,0} = 0, \forall t, \tag{A17}$$

$$p_{l,t,0} - \ \tilde{p}_{l,t,0} = 0, \ \forall l \in L_1, \ \forall t, \tag{A18}$$

$$\sum_{a} E_{lat} \lambda_{l,a,0} - \ p_{l,t,0} = 0, \forall l \in L_2, \forall t \in \left[\underline{T}_l, \bar{T}_l \right], \tag{A19}$$

$$\sum_{a} \lambda_{l,a,0} - 1 = 0, \forall l \in L_2, \tag{A20}$$

$$p_{t,0}^{\text{in}} - p_{t,0}^{\text{out}} + \sum_{\forall i} p_{i,t,0}^{\text{gen}} - p_{t,0} - p_{t,0}^{\text{cha}} + p_{t,0}^{\text{dis}} = 0 \ \forall t, \tag{A21}$$

$$p_{t,0} \geq 0, \ \forall t, \tag{A22}$$

$$p_{l,t,0} \geq 0, \ \forall l \in L_1 \cup L_2, \ \forall t, \tag{A23}$$

$$p_{t,0}^{\text{in}} \geq 0, \ \forall t, \tag{A24}$$

$$p_{t,0}^{\text{out}} \geq 0, \ \forall t, \tag{A25}$$

$$p_{i,t,0}^{\text{gen}} \geq 0, \ \forall i \in I, \ \forall t, \tag{A26}$$

$$p_{t,0}^{\text{dis}} \geq 0, \ \forall t, \tag{A27}$$

$$p_{t,0}^{\text{cha}} \geq 0, \ \forall t, \tag{A28}$$

$$\lambda_{l,a,0} \in \mathbb{B}, \ \forall l \in L_2, \forall a, \tag{A29}$$

$$y_{i,0} \in \mathbb{B}, \ \forall i \in I, \tag{A30}$$

$$y_{ESS,0} \in \mathbb{B}, \tag{A31}$$

$$v_{t,s}^{A17} - v_{t,s}^{A21} - \ u_{t,s}^{A22} = 0, \ \forall t, \ \forall s \in S, \tag{A32}$$

$$-v_{t,s}^{A17} + v_{l,t,s}^{A18} - u_{l,t,s}^{A23} = 0,\ \forall t,\ \forall l \in L_1,\ \forall s \in S, \tag{A33}$$

$$-v_{t,s}^{A17} - v_{l,t,s}^{A19} - u_{l,t,s}^{A23} = 0,\ \forall t,\ \forall l \in L_1,\ \forall s \in S, \tag{A34}$$

$$c_{t,s}^{\text{buy}} + v_{t,s}^{A21} - u_{t,s}^{A24} = 0,\ \forall t,\ \forall s \in S, \tag{A35}$$

$$-c_{t,s}^{\text{sell}} - v_{t,s}^{A21} - u_{t,s}^{A25} = 0,\ \forall t,\ \forall s \in S, \tag{A36}$$

$$\begin{aligned}&\left(c_i^{\text{oper}}/\alpha_i^{\text{gen}} + c_i^{\text{main}}\right) - u_{i,t,s}^{A7} + u_{i,t,s}^{A8} + \left(u_{i,s}^{A10} - u_{i,t,s}^{A11} + u_{i,t,s}^{A12}\right)\\ &+v_{t,s}^{A21} - u_{i,t,s}^{A26} = 0,\ \forall i \in I,\ t = 1,\ \forall s \in S\end{aligned}, \tag{A37}$$

$$\begin{aligned}&\left(c_i^{\text{oper}}/\alpha_i^{\text{gen}} + c_i^{\text{main}}\right) - u_{i,t,s}^{A7} + u_{i,t,s}^{A8} + \left(u_{i,t-1,s}^{A11} - u_{i,t,s}^{A11} + u_{i,t,s}^{A12} - u_{i,t-1,s}^{A12}\right)\\ &+v_{t,s}^{A21} - u_{i,t,s}^{A26} = 0,\ \forall i \in I,\ \forall t = 2,\ldots,22,\ \forall s \in S\end{aligned}, \tag{A38}$$

$$\left(c_i^{\text{oper}}/\alpha_i^{\text{gen}} + c_i^{\text{main}}\right) - u_{i,t,s}^{A7} + u_{i,t,s}^{A8} + \left(u_{i,t,s}^{A11} - u_{i,t,s}^{A12}\right) + v_{t,s}^{A21} - u_{i,t,s}^{A26} = 0,\ \forall i \in I,\ t = 23,\ \forall s \in S, \tag{A39}$$

$$u_{i,t,s}^{A11} = 0,\ \forall i \in I,\ \forall t,\ \forall s \in S, \tag{A40}$$

$$c_{ESS}^{\text{main}} + u_{t,s}^{A14} + \sum_{a=t}^{nT} u_{a,s}^{A16}/\alpha^{\text{dis}} - \sum_{a=t}^{nT} v_{t,s}^{A17}/\alpha^{\text{dis}} + v_{t,s}^{A21} - u_{t,s}^{A27} = 0, \forall t, \forall s \in S, \tag{A41}$$

$$c_{ESS}^{\text{main}} + u_{t,s}^{A14} + \sum_{a=t}^{nT} u_{a,s}^{A16}/\alpha^{\text{dis}} - \sum_{a=t}^{nT} v_{t,s}^{A17}/\alpha^{\text{dis}} + v_{t,s}^{A21} - u_{i,t,s}^{A27} = 0, \forall t, \forall s \in S, \tag{A42}$$

$$c_{ESS}^{\text{main}} + u_{t,s}^{A13} - \sum_{a=1}^{t} \alpha^{\text{cha}} u_{a,s}^{A16} + \sum_{a=1}^{t} \alpha^{\text{cha}} v_{t,s}^{A17} - v_{t,s}^{A21} - u_{t,s}^{A28} = 0,\ \forall t,\ \forall s \in S, \tag{A43}$$

$$c_{ESS}^{\text{main}} + u_{t,s}^{A13} - \sum_{a=t}^{nT} \alpha^{\text{cha}} u_{a,s}^{A16} + \sum_{a=t}^{nT} \alpha^{\text{cha}} v_{t,s}^{A17} - v_{t,s}^{A21} - u_{t,s}^{A28} = 0,\ \forall t,\ \forall s \in S, \tag{A44}$$

$$\underline{P_i} y_{i,s} - p_{i,t,s}^{\text{gen}} \le 0,\ \forall i \in I,\ \forall t,\ \forall s \in S, \tag{A45}$$

$$p_{i,t,s}^{\text{gen}} - \bar{P}_i y_{i,s} \le 0,\ \forall i \in I,\ \forall t,\ \forall s \in S, \tag{A46}$$

$$p_{i,t,s}^{\text{gen}} - P_i^{RES} y_{i,s} \le 0,\ \forall i \in I_{RES},\ \forall t,\ \forall s \in S, \tag{A47}$$

$$p_{i,0,s}^{\text{gen}} - \Delta \bar{P}_i y_{i,s} \le 0,\ \forall i \in I,\ \forall s \in S, \tag{A48}$$

$$\nabla \underline{P_i} y_{i,s} - p_{i,t,s}^{\text{gen}} + p_{i,t-1,s}^{gen} \le 0,\ \forall i \in I,\ \forall t = 2,\ldots,23,\ \forall s \in S, \tag{A49}$$

$$p_{i,t,s}^{\text{gen}} - p_{i,t-1,s}^{\text{gen}} - \Delta \bar{P}_i y_{i,s} \le 0,\ \forall i \in I,\ \forall t = 2,\ldots,23,\ \forall s \in S, \tag{A50}$$

$$p_{t,s}^{\text{cha}} - \bar{P}^{\text{cha}} y_{ESS,s} \leq 0,\ \forall t,\ \forall s \in S, \tag{A51}$$

$$p_{t,s}^{\text{dis}} - \bar{P}^{\text{dis}} y_{ESS,s} \leq 0,\ \forall t,\ \forall s \in S, \tag{A52}$$

$$\underline{\text{E}} y_{ESS,s} - \sum_{i=1}^{t} \left(\alpha^{\text{cha}} p_{i,s}^{\text{cha}} - p_{i,s}^{\text{dis}} / \alpha^{\text{dis}} \right) \leq 0,\ \forall t,\ \forall s \in S, \tag{A53}$$

$$\sum_{i=1}^{t} \left(\alpha^{\text{cha}} p_{i,s}^{\text{cha}} - p_{i,s}^{\text{dis}} / \alpha^{\text{dis}} \right) - \bar{E} y_{ESS,s} \leq 0,\ \forall t, \forall s \in S, \tag{A54}$$

$$p_{t,s} - \sum_{t} p_{l,t,s} = 0, \forall t, \forall s \in S, \tag{A55}$$

$$p_{l,t,s} - \ \tilde{p}_{l,t,s} = 0,\ \forall l \in L_1,\ \forall t,\ \forall s \in S, \tag{A56}$$

$$\sum_{a} E_{lat} \lambda_{l,a,s} - p_{l,t,s} = 0, \forall l \in L_2, \forall t \in \left[\underline{T_l}, \bar{T}_l \right], \forall s \in S, \tag{A57}$$

$$\sum_{a} \lambda_{l,a,s} - 1 = 0, \forall l \in L_2, \forall s \in S, \tag{A58}$$

$$p_{t,s}^{\text{in}} - p_{t,s}^{\text{out}} + \sum_{\forall i} p_{i,t,s}^{\text{gen}} - p_{t,s} - p_{t,s}^{\text{cha}} + p_{t,s}^{\text{dis}} = 0 \forall t, \forall s \in S, \tag{A59}$$

$$p_{i,t,s}^{\text{gen}} - \bar{P}_i y_{i,s} + M^P \left(1 - w_{i,t,s}^{A7} \right) \geq 0,\ \forall i \in I,\ \forall t,\ \forall s \in S, \tag{A60}$$

$$u_{i,t,s}^{B7} \leq M^D w_{i,t,s}^{A7},\ \forall i \in I,\ \forall t,\ \forall s \in S, \tag{A61}$$

$$\underline{P_i} y_{i,s} - p_{i,t,s}^{\text{gen}} + M^P \left(1 - w_{i,t,s}^{A8} \right) \geq 0,\ \forall i \in I,\ \forall t,\ \forall s \in S, \tag{A62}$$

$$u_{i,t,s}^{B8} \leq M^D w_{i,t,s}^{A8},\ \forall i \in I,\ \forall t,\ \forall s \in S, \tag{A63}$$

$$p_{i,t,s}^{\text{gen}} - P_i^{RES} y_{i,s} + M^P \left(1 - w_{i,t,s}^{A9} \right) \geq 0,\ \forall i \in I_{RES},\ \forall t,\ \forall s \in S, \tag{A64}$$

$$u_{i,t,s}^{B9} \leq M^D w_{i,t,s}^{A9},\ \forall i \in I_{RES},\ \forall t,\ \forall s \in S, \tag{A65}$$

$$p_{i,0,s}^{\text{gen}} - \nabla \bar{P}_i y_{i,s} + M^P \left(1 - w_{i,0,s}^{A10} \right) \geq 0,\ \forall i \in I,\ t = 0,\ \forall s \in S, \tag{A66}$$

$$u_{i,0,s}^{B10} \leq M^D w_{i,0,s}^{A10},\ \forall i \in I,\ t = 0,\ \forall s \in S, \tag{A67}$$

$$\nabla \underline{P_i} y_{i,s} - p_{i,t,s}^{\text{gen}} + p_{i,t-1,s}^{\text{gen}} + M^P \left(1 - w_{i,t,s}^{A11} \right) \geq 0,\ \forall i \in I,\ \forall t = 2, \ldots, 23,\ \forall s \in S, \tag{A68}$$

$$u_{i,t,s}^{B11} \leq M^D w_{i,t,s}^{A11},\ \forall i \in I,\ \forall t = 2, \ldots, 23,\ \forall s \in S, \tag{A69}$$

$$p_{i,t,s}^{\text{gen}} - p_{i,t-1,s}^{\text{gen}} - \nabla \bar{P}_i y_{i,s} + M^P \left(1 - w_{i,t,s}^{A12} \right) \geq 0,\ \forall i \in I,\ \forall t\ =\ 2, \ldots, 23,\ \forall s \in S, \tag{A70}$$

$$u_{i,t,s}^{B12} \le M^D w_{i,t,s}^{A12},\ \forall i \in I,\ \forall t\ =\ 2,\ldots,23,\ \forall s \in S, \tag{A71}$$

$$p_{t,s}^{\text{cha}} - \bar{P}^{\text{cha}} y_{ESS,s} + M^P\left(1 - w_{t,s}^{A13}\right) \ge 0, \forall t, \forall s \in S \tag{A72}$$

$$u_{t,s}^{B13} \le M^D w_{t,s}^{A13},\ \forall t,\ \forall s \in S, \tag{A73}$$

$$p_{t,s}^{\text{dis}} - \bar{P}^{\text{dis}} y_{ESS,s} + M^P\left(1 - w_{t,s}^{A14}\right) \ge 0,\ \forall t,\ \forall s \in S, \tag{A74}$$

$$u_{t,s}^{B14} \le M^D w_{t,s}^{A14},\ \forall t,\ \forall s \in S, \tag{A75}$$

$$\underline{E} - \sum_{i=1}^{t}\left(\alpha^{\text{cha}} p_{i,s}^{\text{cha}} - p_{i,s}^{\text{dis}}/\alpha^{\text{dis}}\right) + M^P\left(1 - w_{t,s}^{A15}\right) \ge 0, \forall t, \forall s \in S, \tag{A76}$$

$$u_{t,s}^{B15} \le M^D w_{t,s}^{A15},\ \forall t,\ \forall s \in S, \tag{A77}$$

$$\sum_{i=1}^{t}\left(\alpha^{\text{cha}} p_{i,s}^{\text{cha}} - p_{i,s}^{\text{dis}}/\alpha^{\text{dis}}\right) - \bar{E} + M^P\left(1 - w_{t,s}^{A16}\right) \ge 0, \forall t, \forall s \in S, \tag{A78}$$

$$u_{t,s}^{B16} \le M^D w_{t,s}^{A16},\ \forall t,\ \forall s \in S, \tag{A79}$$

$$u_{it}^{A7}, u_{it}^{A8}, \ldots, u_{it}^{A16} \ge 0, \tag{A80}$$

$$u_{it}^{A22}, u_{it}^{A23}, \ldots, u_{it}^{A28} \ge 0, \tag{A81}$$

$$\begin{aligned}
&\sum_{\forall t}\left[c_t^{\text{buy}} p_{t,0}^{\text{in}} - c_t^{\text{sell}} p_{t,0}^{\text{out}} + \sum_{\forall t}\left(c_i^{\text{oper}}/\alpha_i^{\text{gen}} + c_i^{\text{main}}\right) p_{i,t,0}^{\text{gen}} + c_{ESS}^{\text{main}}\left(p_{t,0}^{\text{cha}} + p_{t,0}^{\text{dis}}\right)\right] + \\
&+ \sum_{\forall i} \alpha_i^{CRF} \pi_i \left(1 - x_{i,0}\right) y_{i,0} + \alpha_{ESS}^{CRF} \pi_{ESS} \left(1 - x_{ESS,0}\right) y_{ESS,0} \le \\
&\sum_{\forall i}\left[c_t^{\text{buy}} p_{t,s}^{\text{in}} - c_t^{\text{sell}} p_{t,s}^{\text{out}} + \sum_{\forall i}\left(c_i^{\text{oper}}/\alpha_i^{\text{gen}} + c_i^{\text{main}}\right) p_{i,t,s}^{\text{gen}} + c_{ESS}^{\text{main}}\left(p_{t,s}^{\text{cha}} + p_{t,s}^{\text{dis}}\right)\right] \\
&+ \sum_{\forall i} \alpha_i^{CRF} \pi_i \left(1 - x_{i,s}\right) y_{i,s} + \alpha_{ESS}^{CRF} \pi_{ESS} \left(1 - x_{ESS,s}\right) y_{ESS,s},\ \forall s \in S
\end{aligned}, \tag{A82}$$

$$p_{t,s} \ge 0,\ \forall t,\ \forall s \in S, \tag{A83}$$

$$p_{l,t,s} \ge 0,\ \forall l \in L_1 \cup L_2,\ \forall t,\ \forall s \in S, \tag{A84}$$

$$p_{t,s}^{\text{in}} \ge 0,\ \forall t,\ \forall s \in S, \tag{A85}$$

$$p_{t,s}^{\text{out}} \ge 0,\ \forall t,\ \forall s \in S, \tag{A86}$$

$$p_{i,t,s}^{\text{gen}} \ge 0,\ \forall i \in I,\ \forall t,\ \forall s \in S, \tag{A87}$$

$$p_{t,s}^{\text{dis}} \ge 0,\ \forall t,\ \forall s \in S, \tag{A88}$$

$$p^{\text{cha}}_{t,s} \geq 0,\ \forall t,\ \forall s \in S, \tag{A89}$$

$$\lambda_{l,a,s} \in \mathbb{B},\ \forall l \in L_2, \forall a,\ \forall s \in S, \tag{A90}$$

$$y_{i,s} \in \mathbb{B},\ \forall i \in I,\ \forall s \in S, \tag{A91}$$

$$y_{ESS,s} \in \mathbb{B},\ \forall s \in S. \tag{A92}$$

Appendix B

Upper bounds on primal and dual variables

For solving a single-level model derived from bilevel programs using KKT conditions, it is important to set appropriate values upper bounds on primal and dual variables, M^P and M^D. This is because, depending on the values of M^P and M^D, the solutions to the original bilevel problem could be cut off, or the efficiency of a solution algorithm could be affected. It should be noted that the appropriate value of M^P is often available because it is related to primal variables and parameters, which are typically bounded. However, M^D is the upper bound on dual variables, so tuning M^D to an appropriate value is a challenging task. Kleinert et al. (2020) prove that in bilevel programming, verifying that a given big-M does not cut off any feasible vertex in the lower level's dual polyhedron cannot be figured out in polynomial time unless P = NP. In addition, they showed computing that a big-M that does not exclude any optimal point of the lower level's dual problem is as hard as solving the original bilevel problem. Nevertheless, we provide the process of tuning big-M empirically and validly in implementing the proposed algorithm for reproducibility as follows.

In our experimental setting, we first determine the tight value of M^P. As we mentioned above, the appropriate value of M^P can be obtained from primal variables and parameters. Let $\tilde{M} \in \mathbb{R}$ be a constant and suppose that $\tilde{M} \geq M^P$ holds. Let there be a feasible region defined by constraints in (A45)–(A59) and (A83)–(A92). From the constraint in (A60), we can get $p^{\text{gen}}_{i,t,s} - \bar{P}_i y_{i,s} + M^P \geq 0$ for every $i \in I$, every t, and given s, by setting the auxiliary binary variable $w^{B7}_{i,t,s}$ to zero. Also, $\tilde{M} \geq \bar{P}_i y_{i,s} - p^{\text{gen}}_{i,t,s}$ holds. Here, $\bar{P}_i \geq \bar{P}_i y_{i,s} - p^{\text{gen}}_{i,t,s}$ is true if and only if $\bar{P}_i$ is non-negative for every i because constraints in (A87) and (A91) stipulate the upper/lower bounds of the first/second terms in the right-hand side of the equation, respectively. Then, the maximum value of $\bar{P}_i$ for every i is the lower bound of $\tilde{M}$ that satisfies the bounds $\tilde{M} \geq \bar{P}_i y_{i,s} - p^{\text{gen}}_{i,t,s}$. Applying these procedures to constraints in (A62), (A64), (A66), (A68), (A70), (A72), (A74), (A76), and (A78), we then obtained $\max_{\forall i}\{\bar{P}_i\}$, $\max_{\forall i}\{P^{RES}_i\}$, $\max_{\forall i}\{\nabla\bar{P}_i\}$, $\max_{\forall i}\{\bar{P}_i\}$, $\max_{\forall i}\{\bar{P}_i + \nabla\bar{P}_i\}$, $\bar{P}^{\text{cha}}$, $\bar{P}^{\text{dis}}$, $\bar{E}$, and $\bar{E}$ as the lower bounds of $\tilde{M}$ in each constraint. Thus, $\max\{\max_{\forall i}\{\bar{P}_i\}, \max_{\forall i}\{P^{RES}_i\},\ \max_{\forall i}\{\nabla\bar{P}_i\}, \max_{\forall i}\{\bar{P}_i + \nabla\bar{P}_i\}, \bar{P}^{\text{cha}}, \bar{P}^{\text{dis}}, \bar{E},\}$ is a correct value of M^P.

Regarding tuning the appropriate value of M^D, the most commonly used technique reported in the technical literature is known as the trial-and-error tuning procedure. This procedure has been used in a number of studies related to electricity grid security analysis (Motto et al., 2005), transmission expansion planning (Jenabi et al., 2013), and strategic bidding of power producers (Zugno et al., 2013). The trial-and-error tuning procedure runs as follows: (1) select initial values

for M^P and M^D; (2) solve the single-level model; and (3) find an i for every s such that $u_{is} = 0$ and $-g_i(\mathbb{x}^L, \mathbb{x}_s^F, \mathbb{y}_s^F) = M^P$. If such as i exists, increase the value of M^P and go to Step (2). Otherwise, go to Step (4) as follows: (4) Find an i for every s such that $u_{is} = 1$ and $u_{is} = M^D$. If such an i exists, increase the value of M^D and go to Step (2). Otherwise, the solution to the single-level model *is assumed* to correspond to the optimal solution of the original bilevel problem. Because we already know the appropriate value of M^P, we only set the initial value of M^D to a sufficiently small value of 50. We ran the trial-and-error procedure on the baseline instance with $B = 50$. When modifying the value of M^D in step (4) of the procedure, it was increased by 50. As a result, the procedure was terminated with a value of 550. However, Pineda and Morales (2019) reported that the trial-and-error procedure may lead to suboptimal solutions for bilevel programs. They demonstrated that the trial-and-error procedure does not guarantee global optimality of the original bilevel problem, showing a counterexample of a simplified bilevel problem. Hence, we set M^D to the value that does not affect the tolerance of the algorithm, that is, $(M^D = 10^4)$, and ran the algorithm to obtain the computational results. The results were compared with the objective value obtained with $M^D = 550$, which is suggested by the trial-and-error procedure, and the same value was recorded. The above process was applied to the two instances with $B = 0$ and $B = 100$. The obtained bounds resulted in 550 and 850. It should be noted that in all computational experiments, including performance testing of the algorithm and sensitivity analysis of instances, we set M^P and M^D to 1000.